ice (-78 °C) in the dark to slow down clustering reactions such as eq 51 and 52.

$$2Fe(CO)_5 \rightarrow Fe_2(CO)_9 + CO \quad (51)$$

$$Fe(CO)_5 + Fe_2(CO)_9 \rightarrow Fe_3(CO)_{12} + 2CO \quad (52)$$

Prior to each use, $Fe(CO)_5$ is opened to the vacuum several times to remove any evolved CO.

Ethylenetetracarbonyliron is synthesized by the method of Murdoch and Weiss.[35] The 300-mL cannister of a Parr pressure reactor is loaded in an argon-purged glovebox with 50 g of $Fe_2(CO)_9$ (Strem) and 125 mL of pentane which has been distilled over sodium benzophenone. The cannister is pressurized to 750 psi with Matheson Research grade ethylene (99.99% min) and stirred at room temperature for 2 days. Periodically, the canister is repressurized to 750 psi as ethylene dissolves and reacts according to eq 53. The resultant green-brown liquid is

$$Fe_2(CO)_9 + C_2H_4 \rightarrow Fe(CO)_4(C_2H_4) + Fe(CO)_5 \quad (53)$$

degassed and most of the pentane is evaporated away. The remaining liquid is fractionally distilled to an icewater cooled receiving flask under a reduced pressure of 10 Torr. The first fraction is $Fe(CO)_5$, which is collected between 24 and 28 °C. The second fraction, collected from 28 to 33 °C, is a yellow-orange mixture of $Fe(CO)_5$ and $Fe(CO)_4(C_2H_4)$. The final fraction is yellow $Fe(CO)_4(C_2H_4)$, which is collected between 32 and 34 °C. This final fraction is thoroughly degassed, transferred to a clean, dry Schlenck tube, and stored over dry ice in the dark. No $Fe(CO)_5$ is detected in the final product by FTIR.

Over time, $Fe(CO)_4(C_2H_4)$ decomposes by forming dodecacarbonyltriiron and ethylene as illustrated in eq 54.

$$3Fe(CO)_4(C_2H_4) \rightarrow Fe_3(CO)_{12} + 3C_2H_4 \quad (54)$$

Thus, $Fe(CO)_4(C_2H_4)$ is opened to the vacuum several times before each use, to remove any free ethylene.

Acknowledgment. This work was supported by the National Science Foundation under Grant No. CHE-86 14702.

Registry No. $CH_2=CH_2$, 74-85-1; $Fe(CO)_3(C_2H_4)_2$, 74278-01-6.

(35) Murdoch, H. D.; Weiss, E. *Helv. Chim. Acta* **1963**, *46*, 1588.

Molecular Modeling of Zeolite Structure. 1. Properties of the Sodalite Cage

M. Mabilia,[†] R. A. Pearlstein,[‡] and A. J. Hopfinger*[‡§]

Contribution from Intersoft Inc., Lake Forest, Illinois 60045, and Department of Medicinal Chemistry and Pharmacognosy and Department of Chemistry, University of Illinois at Chicago, Chicago, Illinois 60680. *Received February 9, 1987*

Abstract: Free-valence geometry molecular mechanics calculations were carried out on a sodalite cage. Energy minimizations were performed as a function of cage oxygen geometry, flexibility of the surface hydroxyl groups, Si:Al composition and bonding topology, and choice of force-field parameters. The major finding is that incorporation of Al atoms into the sodalite cage has little effect on the optimized molecular geometry, but plays a major role on structural stability. As the amount of Al increases, the stability of the sodalite cage also increases. For a fixed Si:Al composition, bonding topologies having localized high density groupings of Al atoms form more stable sodalite cages than those built from random or uniform distributions of Al atoms. Al atoms also increase the ionic character of the sodalite cage. Unique framework oxygen geometries which maximize the stability of a sodalite cage were identified. The optimized sodalite cage structures located on the surface of a zeolite were found to be virtually the same as those within a zeolite framework. Mobile ion-binding calculations, using Na^+ and K^+, indicate that ion-binding strength is most dependent upon the geometry of the cage oxygens. Al atoms play a relatively minor role in ion-binding energetics and specificity.

Zeolites are framework structures usually composed of aluminum, silicon, and oxygen.[1] The zeolite frames constitute porous networks having molecular dimensions. The particular size, shape, and dimensionality of the pores can be controlled by atomic composition and synthetic conditions. Thirty-nine different framework topologies have been observed to date for aluminosilicate zeolites.

Zeolites are increasingly being used in three major commercial applications: catalysis, selective ion exchange, and as molecular sieves and sorbents. Each of these important applications is due to a different component of zeolite structural chemistry. The structural networks in zeolites constitute selective substrates for mobile, nonframework cations, hence the useful ion-exchange properties. The micropores of zeolites are hydrophilic to organophilic depending upon atomic composition. These pores can also be of controlled size(s) and accessibility. Overall, these properties make zeolites effective as sorbents and molecular sieves. The high polarity of bonded atoms in zeolites results in molecular surfaces having highly active sites, again of controlled dimensions. This makes zeolite materials useful in selective catalysis.

At first glance the structural characterization of zeolites would seem straightforward, given their crystalline nature. Unfortunately, these materials have complex bonding topologies and large unit cells. Since diffraction methods yield only a composite average view of a structure, local structural features of zeolites are difficult to discern. Different zeolites can contain common building block structures, additionally making structural differentiation difficult. Perhaps the most significant limitation in applying X-ray diffraction until recently is the small size of synthetic zeolite crystals, normally less than 5 μm in average dimension. Thus, powder diffraction analyses have been the conventional means of distinguishing different zeolites, and, to a lesser extent, determining zeolite structure.[2] However, the loss of structural information inherent to powder diffraction data is usually sufficient to negate detailed refinement of zeolite framework structures.

The net result of these drawbacks and limitations to apply X-ray diffraction methods for the structural resolution of zeolites has

[†] Intersoft Inc.
[‡] Department of Medicinal Chemistry and Pharmacognosy, University of Illinois.
[§] Department of Medicinal Chemistry and Pharmacognosy and Department of Chemistry, University of Illinois.

(1) Newsam, J. M. *Science* **1986**, *231*, 1093.
(2) Barri, S. A. I.; Smith, G. W.; White, D.; Young, D. *Nature (London)* **1984**, *312*, 533.

0002-7863/87/1509-7960$01.50/0

been the use of multiple experimental techniques to characterize the structural chemistry. Most of these methods are indirect measures of molecular geometry, and are also limited by the complexity of the individual zeolite structure. Infrared spectra correlate with local structural framework geometries.[3] Solid-state, magic-angle NMR has been used to deduce the Si:Al ratio in some zeolite structures.[4] The ^{29}Si chemical shifts are sensitive to the geometry of the local environment of this nucleus. For example, there is a correlation between the mean of the bond angles about the four coordinated oxygens to the silicon atom and its chemical shift.[4,5] The ^{29}Si shift is also sensitive to the electron densities of the bonded oxygen atoms and, consequently, indirectly to nonframework species which modify the electron density.[6] X-ray absorption fine structure, Mossbauer spectroscopy, and electron spin resonance spectroscopy have been used to monitor the environments of nonframework cations.[7]

Electron microscopy is widely used in determining sample purity and homogeneity. Corresponding electron diffraction analysis has proven difficult to interpret, but can be used sometimes to define unit cells and symmetries.[8]

Indirect physical measurements of density, sorption, and molecular sieving have been useful in conjunction with spectroscopic methods in postulating zeolite structure.

All of these methods are important in practical studies of zeolites because of the limitations of X-ray diffraction methods to elucidate the molecular geometries of zeolites. Synchrotron radiation spectroscopy[9] and neutron diffraction analysis both offer promise of further elucidating zeolite structure based upon current applications[10] and expected advances in radiation sources.

Various levels and types of molecular modeling and computational chemistry approaches have been applied in the structural analyses of zeolites. One of the first attempts at zeolite modeling was carried out by Dempsey and co-workers.[11] Another early use of computer modeling was the development of a least-squares fit program for zeolite structures.[12] The aluminum distribution over a zeolite framework as a function of fractional composition has also been modeled using Monte Carlo algorithms.[13] Blackwell[14a,b] developed empirical force fields for zeolite frameworks by using model ring structures and fitting force-field parameters to reproduce vibrational properties. Lazarev[15] and Mackenzie[16] also have developed empirical force fields for zeolite structures from experimental data. Catlow[17a,b] and co-workers have combined crystallographic structures and energy minimization techniques to determine properties of silicate minerals with and without exogenous heavy atoms.

Some molecular modeling of zeolite structures has been carried out using computer graphics and fixed-valence geometry molecular mechanics energy calculations.[18] This approach has shown promise in the evaluation of model cation configurations and new framework structures. The methods and strategies employed in these studies are essentially those used in computer-aided drug design,[19] especially in modeling ligand–receptor interactions.

There have also been attempts to explore the catalytic, adsorption, and transport properties of zeolites using semiempirical molecular orbital methods using "small" molecule representations of zeolite structure.[20] The CNDO and INDO methods[21] have been parameterized to carry out calculations involving Al, Si, and some cationic species such as Na^+[20b,22] Very recently No and co-workers[23] have developed free-valence geometry potentials for Na^+ with zeolite structures from X-ray and IR data and energy minimization methods. We plan to use their potentials in an extended transport study to that reported in this paper.

It does not appear that any complete structure optimizations of zeolite geometry have been carried out. Calculations to date have assumed a fixed-valence bond geometry for the zeolite, or have only considered representative single ring structures inherent to zeolites. This paper reports a series of complete structure optimizations of sodalite cages, using free-valence geometry molecular mechanics, in which both Si:Al composition and bonding topology have been varied. In addition, different degrees of structure disordering of the cage oxygens have been investigated as part of the molecular mechanics energy minimization studies. Some binding calculations of Na^+ and K^+ ions to sodalite cages were also carried out. The purpose in doing these calculations was to gain, for the first time, some understanding as to how zeolite stability depends upon chemical structure.

Table I. New Geometric and Force-Field Parameters Needed for Sodalite Cage Modeling

Compression Energy Parameters

	k_1[a]	l_0[b]
Si–O	3.2	1.534
Al–O	2.9	1.720
O–H	4.6	0.942
O–lp	4.6	0.600

Bending Energy Parameters

	k_θ[c]	θ_0[d]
O–Si–O	1.411	106.5
O–Al–O	1.050	109.5
Si–O–Si	0.087	146.5
Si–O–Al	0.310	138.0
Al–O–Al	0.205	138.0
Si–O–H	0.240	115.6
Al–O–H	0.185	108.0
Si–O–lp[e]	0.300	108.0
Al–O–lp	0.330	109.0

Partial Atomic Charges (au) and Dielectric Constant

Si	+1.100	O(Si–O–Si)	−0.527
Al	+1.390	O(Al–O–Si)	−0.575
H	+0.480	O(Si–O–H)	−0.790
		O(Al–O–H)	−0.935
ϵ	5.00		

[a] k_1: stretching constants, in mdyne/Å. [b] l_0: equilibrium bond lengths, in Å. [c] k_θ: bending constants, in mdyne Å/rad^2. [d] θ_0: equilibrium bond angles, in deg. [e] lp stands for the oxygen lone pair.

Methods

The trial sodalite cage structures were constructed using a polyhedra/zeolite generator program (part of the MICROCHEM molecular modeling software system[24] employing algorithms

(3) Rabo, J., Ed. *ACS Monogr.* **1976**, No. 171.
(4) Oldfield, E.; Kirkpatick, R. J. *Science* **1985**, *227*, 1537.
(5) Ramdas, S.; Klinowski, J. *Nature (London)* **1984**, *308*, 521.
(6) Fyfe, C. A., et al. *J. Chem. Soc., Chem. Commun.* **1984**, 514.
(7) Stucky, G. D.; Dwyer, F. G., Eds. *ACS Symp. Ser.* **1983**, No. 218.
(8) Thomas, J. M. In *Proceedings of the Eighth International Congress on Catalysis*; Verlag Chemie: Berlin, 1984; Vol. 1, p 31.
(9) Draj, B., et al., Eds.; *Proceedings of the International Symposium on Zeolites*; Elsevier: Amsterdam, 1985.
(10) Bursil, L. A.; Lodge, E. A.; Thomas, J. M.; Cheetham, A. K. *J. Phys. Chem.* **1981**, *85*, 2409.
(11) Pickert, P. E.; Rabo, J. A.; Dempsey, E.; Schomaker, V. *Proceedings of Third International Congress on Catalysis*; North-Holland: Amsterdam, 1964.
(12) Meier, W. M.; Villiger, H. *Z. Kristallogr.* **1969**, *129*, 411.
(13) Soukoulis, C. M. *J. Phys. Chem.* **1984**, *88*, 4898.
(14) (a) Blackwell, C. S. *J. Phys. Chem.* **1979**, *83*, 3251. (b) Blackwell, C. S. *Ibid.* **1979**, *83*, 3257.
(15) Lazarev, A. N. *Vibrational Spectra and Structure of Silicoates*; Consultants Bureau: New York, 1972.
(16) Mackenzie, K. J. D. *J. Am. Ceram. Soc.* **1972**, *55*, 68.
(17) (a) Catlow, C. R. A.; Cormack, A. N.; Theobald, F. *Acta Crystallogr., Sect. B: Struct. Sci.* **1984**, *40* (3), 195. (b) Parker, S. C.; Catlow, C. R. A.; Cormack, A. N. *Ibid.* **1984**, *40* (3), 200.
(18) (a) Ramdas, S.; Thomas, J. M.; Betteridge, P. W.; Cheetham, A. K.; Davies, E. K. *Angew. Chem., Int. Ed. Engl.* **1984**, *23*, 671. (b) Wright, P. A.; Thomas, J. M.; Cheetham, A. K.; Nowak, A. K. *Nature (London)* **1985**, *318*, 611. (c) Preuss, E.; Linden, G.; Peuckert, M. *J. Phys. Chem.* **1985**, *89*, 2955.
(19) Hopfinger, A. J. *J. Med. Chem.* **1985**, *28*, 1133.
(20) (a) Sauer, J.; Carsky, P.; Zahradnik, R. *Collect. Czech. Chem. Commun.* **1982**, *47*, 1149. (b) Sauer, J.; Zahradnik, R. *Int. J. Quantum Chem.* **1984**, *26*, 793.
(21) Pople, J. A.; Santry, D. P.; Segal, G. A. *J. Chem. Phys.* **1965**, *43*, S129.
(22) Sauer, J.; Deininger, D. *Zeolites* **1982**, *2*, 114.
(23) No, K. T.; Kim, J. S.; Hub, Y. Y.; Kim, W. K.; Jhon, M. S. *J. Phys. Chem.* **1987**, *91*, 740.
(24) MicroChem is a product of Intersoft Inc., 282 East Woodland Rd., Lake Forest, IL 60045.

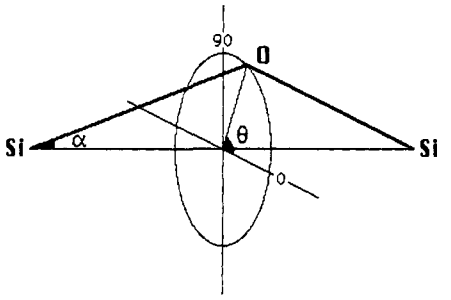

Figure 1. The envelope of locations that a mobile oxygen atom can adopt between two adjacent silicon atoms.

suggested by Pugh.[25] The bond lengths and bond angles used in the initial structures were taken from suggested literature values[26,27] and are reported as part of Table I. The oxygens which bridge to other sodalite cages were terminated with protons. Hence the "surface" of the sodalite cage contains hydroxyl groups.

The sodalite models employed in free-valence geometry calculations include only the framework components: Al, Si, O atoms and surface hydroxyl groups. The presence of cations (one monovalent cation per Al atom) was intrinsically taken into account by adjusting the partial atomic charges of the oxygens bonded to Al atoms, so that the overall charge on the sodalite model is zero, regardless of the Si:Al ratio.

The partial atomic charges were taken from the work of Grigoras[27] in which model structures were optimized at the 3-21G* ab initio level. These charges, adjusted as mentioned above, are also given in Table I. Grigoras found that a "molecular dielectric", ϵ, of 5, in conjunction with the partial charges and force-field parameters found from the ab initio level calculations best reproduced the ab initio optimized structures for an Allinger molecular mechanics model.[28] Thus, we set $\epsilon = 5$ in the structure calculations reported here since an Allinger-like force field was used in our calculations—the MMFF force field in Chemlab-II.[29]

Some of the requisite bond stretch and bond angle bending constants were also taken from the work of Grigoras.[27] These force-field parameters are included in Table I. Some other force fields, as mentioned earlier, have also been reported for zeolite structures.[14-16] We have not used force constants from any of these force fields in order to preserve self-consistency in the calculations. That is, only force constants derived in the same manner as other force constants using the MMFF force-field representation are used in the structure calculations. It is satisfying to note consistency among the force constants derived by different workers. For example, the bond stretch constant found by Blackwell[14a] for the Si–O bond is 3.4756 mdyn/Å while that of Grigoras[27] is 3.2 mdyn/Å. The number of significant numbers in Blackwell's force constant is needed to empirically reproduce the vibrational spectra of zeolite structures.

It should be noted (see Table I) that the bond angle bending constant for O–Al–O is more smaller than that for O–Si–O. Also, the Si–O–Si bond angle bending constant is smaller than all other bond angle bending constants. Torsional barrier potentials were available and included in the energy calculations. However, this energy term is relatively constant because torsional deformations are small in the highly constrained zeolite framework.

Oxygens belonging solely to the sodalite cage can assume a variety of locations relative to one another and the relatively stationary silicon/aluminum atoms. This behavior was quite apparent after analyzing the first few energy minimization calculations on all silicon sodalite cages. The silicon atoms had a composite mean displacement of atomic position of less than 3% the corresponding composite mean displacement of the oxygen atoms. Thus, we had to devise a method of generating different initial oxygen geometries in order to be able to evaluate the role of this geometric factor on sodalite stability. An oxygen atom can be located anywhere on the perimeter of the base of a cone generated by sweeping the bond vector of an Si–O bond through an angle α as shown in Figure 1. The angle α is determined by the Si–O bond length and by the Si–O–Si bond angle. The specific location of an oxygen atom is defined by an angle θ (see Figure 1). A reference position, $\theta = 0°$, was defined as that location in which the oxygen is in a plane which bisects the solid angle formed by two adjacent faces (whose common edge is the Si–Si vector shown in Figure 1) and directed toward the center of the cage. $\theta = 180°$, therefore, corresponds to a location on the same bisector plane, but away from the cage center.

Clearly, the number of oxygen configurations for a sodalite cage is very large owing to the possible combinations of different θ values. Some configurations of oxygen geometries are not possible because of loss of tetrahedral symmetry about the silicon and/or aluminum atoms.

Overall, the large number of possible oxygen geometries was sampled by carrying out energy minimization calculations on representative initial structures having varying degrees of oxygen geometry disorder. The energy minimization calculations involved free-valence geometry modeling, and were carried out using the MMFF option of Chemlab-II,[29] which is a modified form of the Allinger MM2 force field.[28]

Oxygen geometry disorder, β, was measured in terms of the sum of the standard deviations in the distances between first and second nearest-neighbor oxygen pairs over the sodalite cage.

$$\beta = \sum_{i\ \text{1st NN}} \sqrt{\frac{(\bar{d}_1 - d_i)^2}{N_1}} + \sum_{j\ \text{2nd NN}} \sqrt{\frac{(\bar{d}_2 - d_j)^2}{N_2}} \qquad (1)$$

In eq 1 "i 1st NN" refers to the ith first nearest oxygen neighbor pair, d_1 is the average first nearest oxygen neighbor pair distance, d_i is the ith first nearest oxygen neighbor pair distance, and N_1 is the number of first nearest oxygen neighbor pairs. The corresponding indexes in the second term of eq 1 have the same meanings as those in the first term, but refer to second nearest oxygen neighbor pairs.

Different Si:Al compositions were also investigated. These studies were selected to evaluate the role of silicon vs. aluminum upon oxygen mobility, and, overall, sodalite cage stability.

Sodalite Si to Al composition was considered in terms of molecular stability in two ways. First, the amount of Al was varied from 0 to a ratio of 1:1 which is the maximum according to Loewenstein's rule.[30] Secondly, for a fixed Si to Al composition, the topological distribution of Al was varied over the sodalite cage. Again, Loewenstein's rule was used as a constraint. Each resulting sodalite cage of a particular chemical structure was optimized using free-valence geometry molecular mechanics.[28,31]

An attempt was made to simulate a sodalite cage embedded in a complete zeolite framework. This was done by freezing the movement of the surface hydroxyl oxygens during energy minimization and, in some calculations, by deleting the partial charges on the hydroxyl protons and assigning the hydroxyl oxygens partial charges which kept the total sodalite cage charge at zero. This was considered to mimic the situation of steric and electrostatic interactions of sodalite neighbors packed symmetrically about a central sodalite cage, as in SOD framework.[1] In essence, there should be an interaction cancellation effect due to competing atoms within a sodalite cage adjacent to the "central" cage and between cages bonded to the "central" cage. Moreover, the zeolite framework is assumed to be the same over all intrasodalite cage

(25) Pugh, A. *Polyhedra*; University of California Press: Berkeley–Los Angeles, CA, 1976.
(26) Geisinger, K. L.; Biggs, G. V.; Navrotsky, A. *Phys. Chem. Miner.* **1985**, *11*, 266.
(27) (a) Grigoras, S. "Molecular Mechanics Parameters for Organo-Silicon Compounds Calculated from Ab Initio Computations", *J. Phys. Chem.*, submitted for publication. (b) GAUSSIAN-82, Release A VAX Version, Sept 1983, is available from Professor John Pople, Chemistry Department, Carnegie Mellon University, 4400 Fifth Ave., Pittsburgh, PA 15213.
(28) Allinger, N. L. *J. Am. Chem. Soc.* **1977**, *99*, 8127.
(29) Pearlstein, R. A. *Chemlab-II Users' Guide*; Chemlab, Inc.: 1986.
(30) Loewenstein, W. *Am. Mineral.* **1954**, *39*, 92.
(31) Hopfinger, A. J. *Conformational Properties of Macromolecules*; Academic Press: New York, 1973.

Table II. The Lennard-Jones 6–12 Nonbonded Potential Parameters for Interactions Involving Na^+ and K^+

6–12 function: atom pair (ij)	$U_{ij} = -A_{ij}/r_{ij}^6 + B_{ij}/r_{ij}^{12}$	
	A_{ij} (kcal·Å^6/mol)	B_{ij} (kcal·Å^{12}/mol)
Na^+···Si	176.46	131 554.8
Na^+···Al	164.98	34 267.2
Na^+···O	91.31	9 988.8
Na^+···H	41.25	2 796.7
K^+···Si	671.24	903 864.6
K^+···Al	627.60	268 708.7
K^+···O	347.34	84 543.8
K^+···H	156.93	25 180.7

Table III. Results of MMFF Calculations for All-Si Sodalite Structures[a]

structure	initial total energy	iteration no. 5 steric energy	final total energy
0	1269.01	could not be optimized	
30	1541.24	could not be optimized	
60	1658.51	could not be optimized	
90	2464.94	could not be optimized	
120	3187.18	could not be optimized	
140	2359.23	−104.05	−580.18
150	2032.62	−263.24	−753.16
180	778.86	−450.21	−739.59
210	370.75	−429.86	−735.20
240	225.81	−689.52	−758.29
270	−224.63	−768.33	−789.85
280	−311.84	−767.81	−787.47
290	−289.01	−758.98	−775.55
300	−144.58	−726.11	−765.62
330	702.88	−639.11	−737.87
350	1114.92	−551.38	−755.93
random	−144.65	−748.97	−770.73

[a] The total cage energy values are in kcal/mol. All hydroxyl oxygens were held fixed. The bottom structure (random) corresponds to randomly generated values in the angle θ (defined in Figure 1) for each oxygen in the cage. All energies are in kcal/mol.

calculations so that the modeling energy is effectively a constant.

Lastly, we investigated the interaction of Na^+ and K^+ with the surface of a hydroxylated sodalite cage using both fixed- and free-valence geometry optimizations. The overall purpose of these calculations was to see how the oxygens respond to the exogenous chemical species. Different oxygen geometries, as determined from structure optimizations of all Si cages, were used as initial structures in the intermolecular calculations. Optimized cage structures for some of the Si:Al compositions were also considered as substrates for Na^+ and K^+. Valence geometry was held fixed for the cage-ion studies and the mobile ions were driven into and through the sodalite cages using the 12-membered ring faces as entry points. The Na^+ and K^+ ions were treated as spherically symmetric and possessing unit positive point charges at their geometric centers. The Na^+···X and K^+···X, where X is Si, Al, or O, nonbonded potentials were taken from the database in Chemlab-II.[29] These potentials were derived from a method employing a modified Slater–Kirkwood equation and a contact-distance constraint.[32] The potentials are listed in Table II. No and co-workers[23] have reported a free-valence geometry field for the interaction of Na^+ with zeolite structures (Si, Al, and O). We are fitting their potentials to the functional representation in MMFF.[29] Once this is completed, we plan to repeat the Na^+–sodalite cage energy calculations.

The intermolecular potential energies along the path through the cage are given by the sum of the electrostatic and Lennard-Jones (6–12) atom-pair potentials.[31] These calculations were carried out using the PROBE option of Chemlab-II.[29]

Results

The energies of optimized all-silicon sodalite units are reported in Table III for different oxygen geometries. The positions of the hydroxyl oxygens were held fixed during minimization. This situation should approximate the structural constraints experienced by a sodalite cage embedded within a zeolite framework (e.g., the central cage in a SOD zeolite). Clearly, only a small sample of possible oxygen geometries has been considered. However, it is evident that sodalite cage energy is quite sensitive to oxygen geometry. The first few structures (0 through 120) in Table III could not be optimized. As the high initial energy values suggest, their geometries are bad because of highly distorted tetrahedral symmetry around silicon atoms. Figure 2 shows a schematic representation of initial locations of frame oxygens as a function of the angle θ previously defined (see Methods). The heavy-shaded area (between 350 and 140) corresponds to starting geometries that are high in energy and in most cases could not be optimized. The light-shaded area represents the geometries which yielded the lowest optimized minimum energy conformations. Three sample structures are also reported to illustrate the geometric

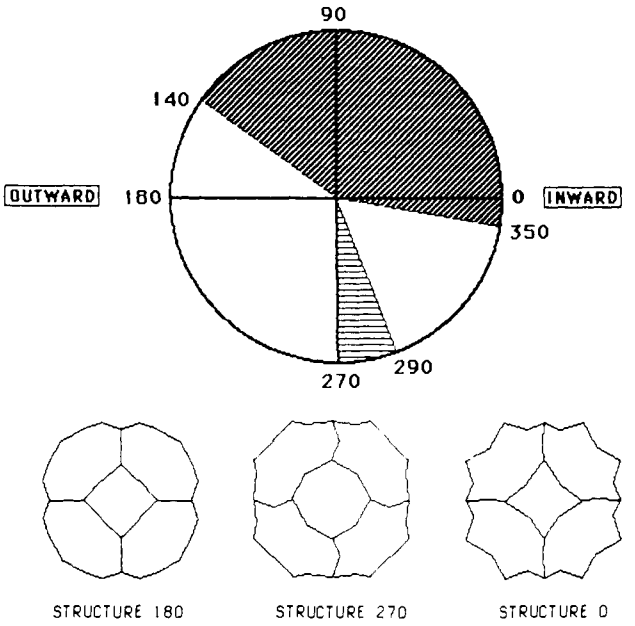

Figure 2. Schematic representation of initial locations of frame oxygens in a sodalite cage before molecular mechanics optimization using MMFF: ///, starting geometries in this range could not be optimized; ≡, starting geometries in this range yielded the lowest minimum energy structures. See the text for definitions of inward and outward.

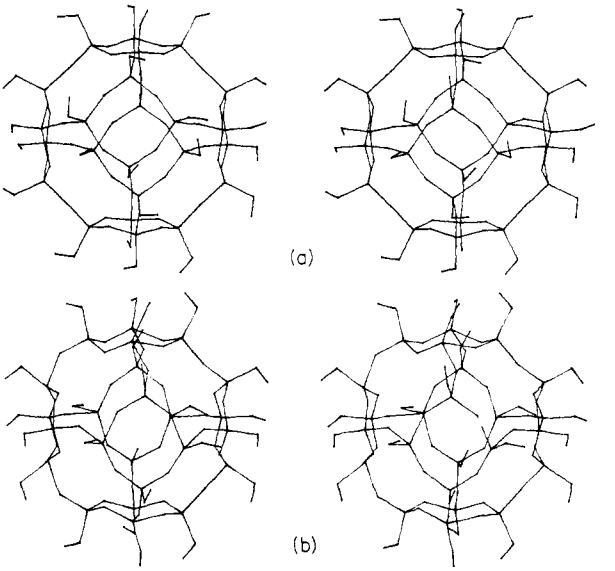

Figure 3. (a) Stereo stick representation of an optimized all-silicon sodalite cage. (b) Stereo stick representation of a slightly distorted 1:1 Si:Al sodalite cage after optimization.

(32) Scott, R. A.; Scheraga, H. A. *J. Chem. Phys.* **1966**, *45*, 2091.

Table IV. Results of MMFF Calculations for Structure 270 (All-Si Sodalite Cage)[a]

	total	compr	bend	str-bnd	van der Waals 1,4	van der Waals other	tors	dipole or Coulombic
a	531.33	27.07	277.37	-27.25	-31.35	-33.50	301.99	17.00
b	-370.03	25.34	270.91	-24.69	-31.66	-33.84	294.66	-870.76
c	-789.85	26.02	270.07	-25.03	-31.71	-33.82	297.60	-1292.99

[a] The motions of all hydroxyl oxygens were restricted. All energies are in kcal/mol. In the first column, a denotes dipole potential with full partial atomic charges on the hydroxyls; b, coulomb potential with hydroxyl proton charges set to zero and hydroxyl oxygen charges adjusted to set the total charge to zero; c, coulomb potential with full partial atomic charges on the surface hydroxyls.

Table V. MMFF Energy Components for Structure 270 (All-Si Sodalite Cage)[a]

	total	compr	bend	str-bnd	van der Waals 1,4	van der Waals other	tors	electr
all	-789.85	26.02	270.07	-25.03	-31.71	-33.82	297.60	-1292.99
some	-794.60	27.01	267.55	-26.03	-31.65	-34.07	296.31	-1293.71
none	-797.75	28.46	265.09	-27.15	-31.61	-34.36	296.27	-1294.45

[a] "None", "some", and "all" refer to the number of hydroxyl oxygens whose motions were restricted. In particular, "some" mimics one "surface" sodalite unit belonging to SOD or LTA zeolites and "all" mimics the "central" sodalite cage on SOD zeolites. All energies are in kcal/mol.

Table VI.

a. Results of Free-Valence Geometry Molecular Mechanics Calculations for Structure 270 Composed of Different Si:Al Compositions[a]

Si:Al	total	compr	bend	str-bnd	van der Waals 1,4	van der Waals other	tors	electr
24:0	-370.03	25.34	270.91	-24.69	-31.66	-33.84	294.66	-870.76
5:1	-457.51	34.46	253.65	-31.28	-28.89	-34.43	294.43	-945.45
2:1	-524.30	48.87	254.06	-37.39	-26.98	-34.89	293.39	-1021.36
1:1	-691.19	42.84	169.58	-60.22	-21.21	-33.08	298.45	-1087.36

b. Total Energies for Different Topological Distributions of Al (Under the Same Conditions Described Above) for the 3:1 Ratio of Si:Al

Si:Al	description	total energy (kcal/mol)
3:1	local high density of Al atoms	-531.72
3:1	randomly distributed Al atoms	-510.27
3:1	equally distributed Al atoms	-494.76

c. Oxygen Geometry Disorder Index, β, for Different Si:Al Compositions[b]

Si:Al	total energy (kcal/mol)	S_1	S_2	β
all Si	-370.03	0.045	0.405	0.450
5:1	-457.51	0.127	0.460	0.586
3:1	-531.72	0.162	0.532	0.694
2:1	-524.30	0.177	0.483	0.660
1:1	-691.19	0.210	0.616	0.826

[a] All hydroxyl oxygens were held fixed during the minimization. The partial atomic charges on hydroxyl protons were set to zero and charges on hydroxyl oxygens were adjusted to maintain the total charge at zero. The Al "randomly" distributed over the sodalite cage for the 5:1, 3:1, and 2:1 compositions. All energies are in kcal/mol. [b] $\beta = S_1 + S_2$ where S_1 and S_2 are the standard deviations in the distances of first and second, respectively, nearest-neighbor oxygen pairs.

diversity due to oxygen locations.

The lowest minimum energy conformation was found using structure 270 whose starting geometry corresponds to frame oxygens approximately on the planes of the sodalite faces. The optimized structure (shown in stereo in Figure 3a) is characterized by Si–O bond lengths between 1.604 and 1.631 Å, O–Si–O bond angles between 104 and 113°, Si–O–Si bond angles (for any adjacent 8- and 12-membered faces) between 151 and 156°, and Si–O–Si angles (for any two adjacent 12-membered faces) between 171 and 174°. The bigger pore has a minimum diameter of 2.34 Å.

The main difference between structure 270 and its optimized conformation is that the former has a smaller Si–O–Si bond angle (146.5°) for any two adjacent 12-membered faces. Nevertheless, the two structures (initial and optimized) are very similar as can be seen by molecular superposition.

A concern when performing molecular mechanics calculations on a highly polar system like a sodalite cage is the effect of the electrostatic potential energy on the relative stabilities of the minimum energy structures. In order to test this effect, we carried out structure optimizations in which the Coulombic energy contribution was replaced by a dipole interaction energy. The results are reported in Table IV.a for an all-silicon sodalite unit (from structure 270). The results of molecular mechanics structure optimization using a different set of partial atomic charges for the hydroxyl groups are also reported in Table IV.b. The partial charges on the protons were set to zero and those on the hydroxyl oxygens were adjusted to maintain the total charge at zero. Though the absolute energies are quite different under the different conditions, all other energy contributions are relatively constant and the optimized geometries obtained in all cases are virtually identical.

Sodalite cages on the "surface" of a framework, as opposed to "central" cages which are embedded in a framework, experience less structural constraints and, therefore, might undergo some deformations with resulting partial loss of symmetry. In order to test this hypothesis, the position of hydroxyl oxygens, which would be bonded to other sodalite cages in SOD or LTA frameworks,[1] were held fixed while the remaining hydroxyl oxygens were allowed to be free. Structure optimization under these constraints, using structure 270 as a starting geometry, results in negligible geometric deformations and slightly more favorable energetics. Similar results can be achieved for an isolated sodalite cage where all atoms are allowed to move freely. No loss of symmetry is observed, and the optimized structure is almost perfectly superimposable upon each of the structures in which all and some of the hydroxyl oxygens were anchored. The energetics related to these results are reported in Table V.

Table VII. Effect of Parameterization of the Si···X and Al···X (X = Si, Al, O) Nonbonded Potential Functions upon the Relative Stability of Sodalite Units of Three Different Si:Al Compositions[a]

Si:Al	r_{Si}	p^*_{Si}	r_{Al}	p^*_{Al}	total energy
24:0	2.25	0.14	2.34	0.12	-370.03
24:0	2.30	0.07	1.65	0.43	-369.09
3:1	2.25	0.14	2.34	0.12	-531.72
3:1	2.30	0.07	1.65	0.43	-506.81
1:1	2.25	0.14	2.34	0.12	-691.19
1:1	2.30	0.07	1.65	0.43	-666.78

[a] The van der Waals radius, r, is expressed in Å; the depth of the potential well, p^*, and the total energy are in kcal/mol.

The optimized structure energies for different Si:Al compositions are reported in Table VI.a. The 1:1 ratio of Si:Al corresponds to the maximum number of aluminum atoms that can be placed in a sodalite cage such that Loewenstein's rule[30] is satisfied. All hydroxyl oxygens were held fixed during the optimization. Partial atomic charges on hydroxyl protons were set to zero and partial charges on hydroxyl oxygens were adjusted to keep the total charge at zero. The results obtained under these conditions indicate that sodalite cage relative stability is highly dependent upon the Si:Al ratio, irrespective of the oxygen geometry. As the aluminum content increases, the relative conformational stability of the sodalite cage increases. An analysis of the individual energy contributions to the total cage energy indicates that the electrostatic term is mainly responsible for the enhanced conformational stability of sodalite cages having large aluminum contents. The compression energy acts to destabilize sodalite cages of high aluminum content. Other energy contributions are relatively constant as a function of Si:Al composition. Though aluminum atoms tend to increase the relative stability of the cage, they are also responsible for local geometric deformations. For example, a loss of tetrahedral symmetry, especially about some of the aluminum atoms, can be observed. Further investigations are required to determine if such deformations are due to limitations inherent to the minimization procedure, or might be a function of the force-field parameterization. The bond angle bending constant for O–Al–O is smaller than that for O–Si–O; see Table I.

For a fixed Si:Al composition it is also of interest to know how sensitive the cage energy is to the bonding topological distribution of aluminum atoms. Table VI.b. contains the total cage energies for different bonding topological distributions of aluminum for the 3:1 Si:Al ratio. The cage energy, for a fixed composition, is moderately sensitive to bond topological distribution. In particular, it appears that local higher density of aluminum atoms (as opposed to Al atoms equally distributed on the cage) yields energetically more favorable structures.

The behavior of the order/disorder of the oxygen geometry as a function of Si:Al composition is reported in Table VI.c using β (see eq 1) as an order parameter. The data in Table VI.c suggest that the disorder in the cage oxygen geometry increases with an increase in aluminum content. An analysis of the first and second nearest-neighbor (S_1 and S_2) distance deviation terms forming β suggests both local (S_1) and longer-range (S_2) disordering occurs as aluminum content increases. It is not possible to discern to what extent, if any, the oxygen geometry disordering contributes to increasing the relative stability (lowering the conformational energy) of the sodalite cage as Al content is increased.

A major concern when performing molecular mechanics calculations is how dependent the results (i.e., energy values) are upon the parameterization. This is a particularly sensitive issue for silicon and aluminum where the force-field parameters are not well characterized because of the large sizes of these atoms and varying orbital configurations they can adopt in different bonding environments. We have attempted to partially evaluate the sensitivity of the relative stability of sodalite cage geometries for two different parameterizations of the Si···Si and Al···Al nonbonded potential functions. The results are presented in Table VII where r is the van der Waals radius, and p^* represents the depth of the potential well. The Slater–Kirkwood approximation[32] has been used to derive the heteroatom pair interactions, Si···X (X = Al, O) and Al···X (X = Si, O). The cage energies reported in Table VII suggest that the relative stabilities of the sodalite cages are relatively insensitive to moderate changes in nonbonded potential parameterization, and trends in relative stability as a function of Si:Al composition are conserved for different parameterizations.

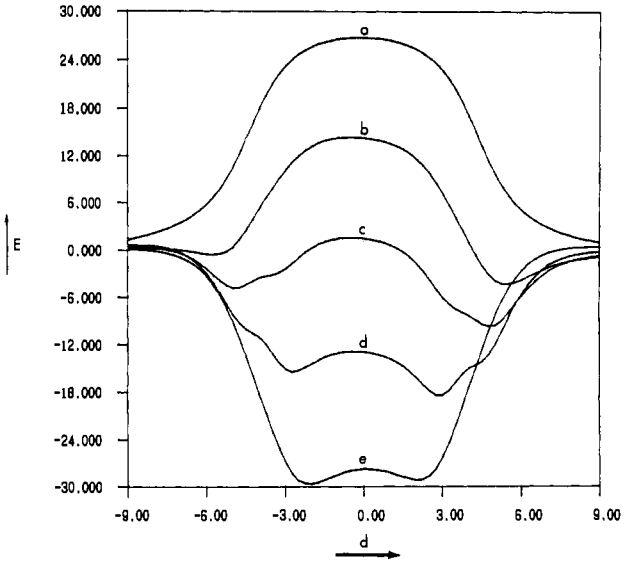

Figure 4. The all-silicon cage–Na^+ interaction energies as a function of Na^+ distance from the center of the cage, for different starting oxygen geometries (see Table III and Figure 2): (a) 180, (b) 240, (c) 270, (d) 300, (e) 0. The distance vector passes through the center of a 12-membered ring face and the center of the cage.

It was not possible to fully test how structurally flexible the sodalite cages are in the presence of exogenous agents. Many valence geometry force-field constants involving Na^+ and K^+ are not available although No et al.[23] have recently reported a Na^+–zeolite force field. Consequently, our initial intermolecular modelling studies employed a fixed-valence geometry constraint. The Na^+ and K^+ ions were driven through different optimized geometries of sodalite cages using the centers of 12-membered faces as entry and exit points.

Figure 4 shows a series of plots of cage–Na^+ interaction energy, E (coulombic electrostatic plus Lennard-Jones 6–12), as a function of the distance, d, from the center of the cage for different nonoptimized oxygen geometries. The curves are not perfectly symmetric with respect to $d = 0$ because of the arbitrary orientations of hydroxyl protons. The top curve (a) corresponds to structure $\theta = 180°$ where the oxygen atoms are on the outside of the cage (see Figure 2). This geometry accounts for the relatively high and broad energy barrier. A Na^+ ion located at the center of the cage, $d = 0$, would experience a strong repulsion generated by silicon atoms, positively charged and closer to the Na^+ than the cage oxygens. The bottom profile (e) corresponds to structure $\theta = 0°$ where the oxygen atoms are located on the inside of the cage. Hence, a relatively strong attraction would be exerted on a Na^+ ion at the center of the cage by the cage oxygens. The middle curve (c) was obtained for structure $\theta = 270°$ and corresponds to oxygen atoms located more or less on the surfaces of the cage. The barrier is much lower and the two minima regions suggest a favorable interaction (mainly of an electrostatic nature) with Na^+ centered above a 12-membered face.

Cage–Na^+ energy profiles are shown in Figure 5 for sodalite units with the same starting oxygen geometries described above, but after structure optimization. All of the interaction energy curves share the same analytical shape characterized by two minimum energy wells and a central barrier. The difference in energy between the barriers for different optimized oxygen geometries is much smaller (within 4 kcal/mol) for the optimized sodalite cage structures than the corresponding initial trial structures (more than 50 kcal/mol). These results, as well as a

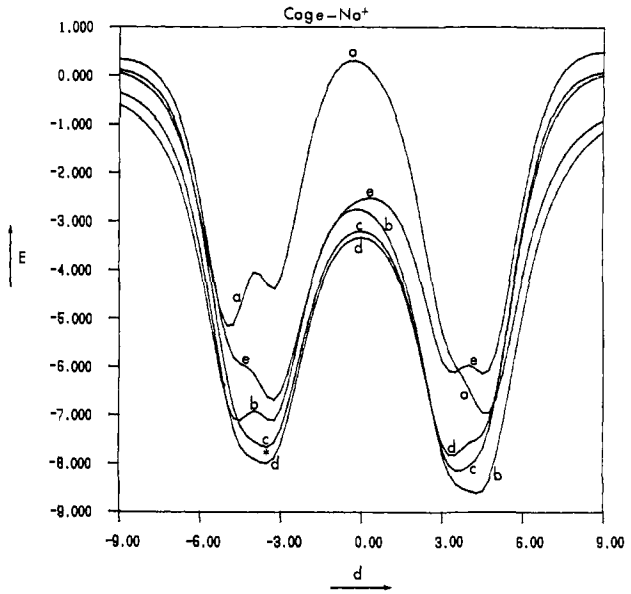

Figure 5. Same as Figure 4 but for optimized structures.

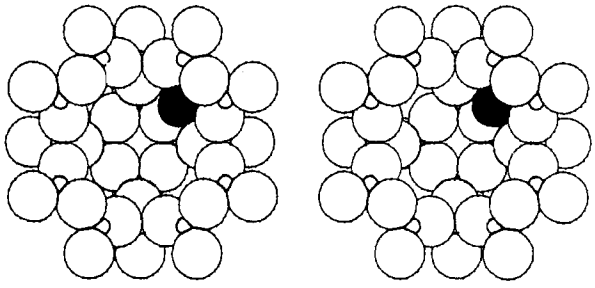

Figure 6. Space-filling stereoview into an optimized all-silicon sodalite unit with a bound Na^+ located as a lightly filled-in ball.

visual analysis of the optimized structures, suggest that symmetry and positional differences in starting oxygen geometries are averaged during energy minimizations, yielding an envelope of conformations which share a common oxygen topology. Common oxygen topology, in turn, significantly modifies the cage–ion interaction energy profiles.

Some of the interaction energy profiles in Figure 5 have pairs of major energy wells, each of which shows two separate subminima corresponding to Na^+ centered on a 12-membered face, interacting with 6 oxygens, toward the outside and, respectively, the inside of the sodalite cavity. Figure 6 depicts a clipped space-filling stereoview into the optimized all-Si sodalite cage. The big van der Waals spheres are cage oxygen atoms and the smaller ones represent silicon atoms, shielded by tetrahedra of the bonded oxygens. The Na^+ ion interacting with the cage, and centered on one of the faces, corresponds to the minimum energy state marked with an * in Figure 5. Finally, for any given energy profile in Figure 5, the difference in energy between the bottom of the well and the top of the central barrier is only about 5 kcal/mol. Of course, these energies are dependent upon the molecular dielectric which is 5 in the work reported here.

Similar cage–Na^+ curves are shown in Figure 7 for two optimized sodalite units with Si:Al ratios of 2:1 and 5:1 and for an optimized all-silicon sodalite unit (derived from structure 270) used as a reference. The asymmetry in the potential curves for the 2:1 and 5:1 cages is due to a skewed distribution of Al atoms on one side of the cage (for $d < 0$). This results in both a structural and electrostatic asymmetry contribution to the cage potential energy.

Figures 8 and 9 depict the corresponding plots to Figures 5 and 7, respectively, for the K^+ ion. The most striking difference between these and the previous cage–Na^+ energy profiles resides in the relatively high-energy barriers when the ion passes through the planes of the faces. These barriers are due to the larger ionic

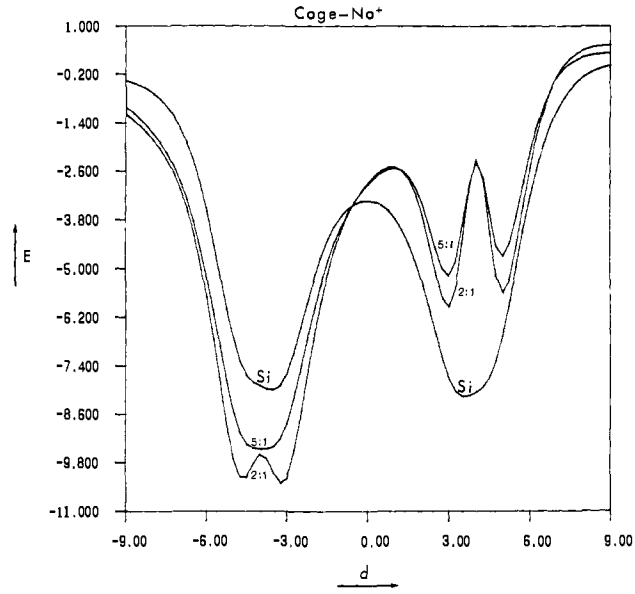

Figure 7. Same energy profiles as in Figure 4 but for optimized all-silicon, 2:1 and 5:1 Si:Al ratios sodalite units.

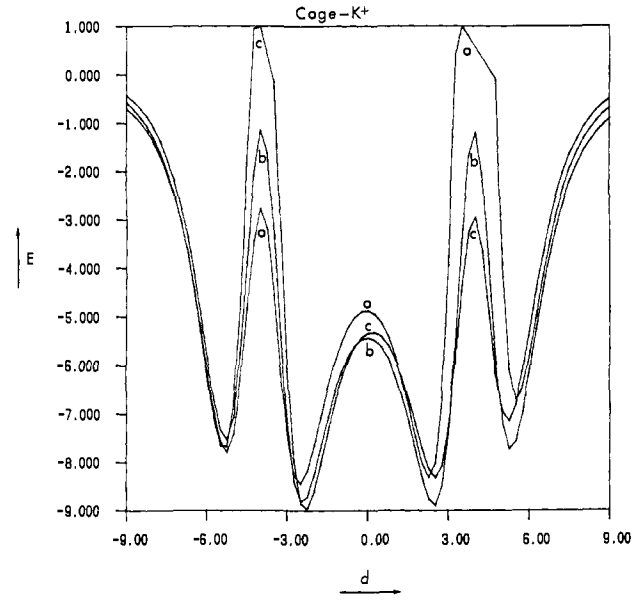

Figure 8. Same as Figure 5 but for cage–K^+ interactions: (a) structure 240, (b) 270, (c) 300.

radius of K^+ (1.44 Å) compared to Na^+ (1.12 Å). This results in a steric repulsion between K^+ and the six oxygens which constitute one of the larger pores (its minimum diameter is 2.34 Å).

As a general finding, the inclusion of aluminum atoms in the sodalite unit appears to have minimal effect on the ion–cage interaction energy for both Na^+ and K^+ ions. A partial lack of symmetry in the profiles of Figures 7 and 9 is quite evident. This fact can be attributed, as mentioned above, to local geometry distorsions of the hydroxyls introduced during the optimization procedure, and to the presence of aluminum atoms which are not symmetrically distributed over the cage. The absolute interaction energies, for a given sodalite unit and ion, are quite similar for both Na^+ and K^+.

Discussion

The most important finding from this study is the role that the Al atoms play in the structure and stability of the sodalite cage. The incorporation of Al atoms into the sodalite cage has a minimal effect on the molecular geometry of the heavy atoms cage structure irrespective of the oxygen geometry and bonding topology of the Si and/or Al. However, the conformational stability (absolute minimum energy) of the sodalite cage increases as Al is added

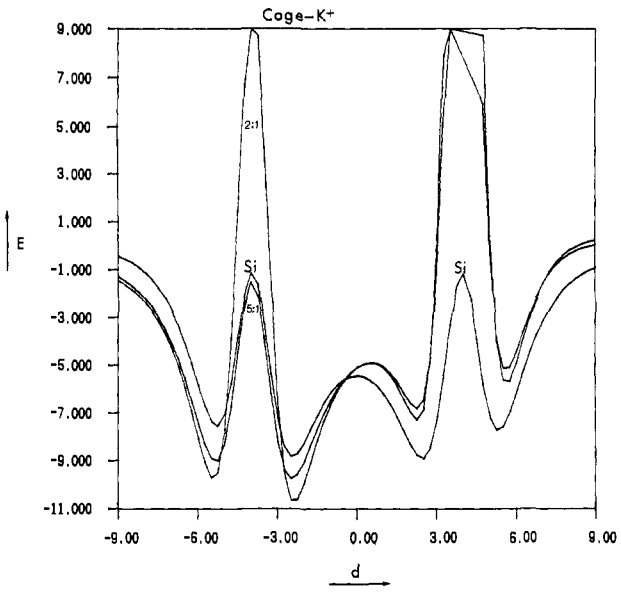

Figure 9. Same as Figure 7 but for cage-K^+ interactions.

to the sodalite cage. The decrease in repulsive electrostatic interactions with increasing Al content is the primary source of this increase in sodalite cage stability. An inspection of the partial charge densities in Table I suggests that the Al atoms enhance the ionic nature of the sodalite cage. That is, the magnitudes of the partial charge densities on both the aluminum atoms and adjacent oxygens are respectively greater than for the Si atoms and their adjacent oxygens. Thus, we conclude that the stability of a sodalite cage increases as its ionic character increases. This observation for the entire sodalite cage appears to persist down to local geometries within a sodalite cage. The data reported in Table VI.b suggest, for a fixed Si:Al ratio, that those bonding topological distributions having a locally dense makeup of Al atoms have a lower (more stable) sodalite cage energy than random and/or uniform distributions of Al atoms. A locally dense distribution of Al atoms results in a correspondingly high local ionic character. It is tempting to suggest that such locally dense distributions of Al atoms preferentially form because of the favorable energetics and, in turn, are responsible for some of the useful catalytic properties of zeolites.

While experimental findings are somewhat ambiguous, the common consensus is that these data indicate that the sodalite cage is *destabilized* with increasing Al content. This is not consistent with computational studies reported here. There are a few possible explanations for this apparent discrepancy. One is that the calculations are in error. Most likely the electrostatic energy contribution would be the major source of the error. A second explanation is that long-range interactions arising between atoms of different sodalite cages are important and work, in composite, to destabilize the zeolite framework with increasing Al composition. Another explanation is that the experimental findings are not reliable. However, the more likely explanation is that two different energies are being determined by experiment and by computation. The calculations involve computing conformational energy, while the experiments measure the bond energy plus the conformational energy. The Si–O bond energy is larger than the Al–O bond energy. Thus, increasing Al content should decrease the total bond energy of the sodalite cage. It would appear that the loss in bond energy outweighs the calculated gain in conformational energy as Al content increases according to experimental findings.

The cage oxygens have a large amount of intrinsic geometric freedom (see Figure 1). However, an analysis of the results given in Table III, and portrayed in Figure 2, indicates that only a small range in possible oxygen geometries, as measured by the angle θ, leads to sodalite cage structures that are within 20 kcal/mol of the most stable structure ($\theta = 270°$). Thus, the sodalite cage is more rigid than might be expected from the possible intrinsic mobility of the cage oxygens.

Table III also contains computational information that may be critical in extending free-valence geometry molecular mechanics calculations to larger zeolite systems. It generally takes about 220 iterations for convergence to be realized in an energy minimization of a sodalite cage. A comparison among the initial total energies, steric energies after five iterations, and the final total energies (see, for example, Table III) indicates that over 90% of the energy minimization, and corresponding structure optimization, is realized by the end of the fifth iteration. This suggests that over the next 215 iterations a large number of small, relatively inconsequential, atomic movements occur. Perhaps the convergence criteria can be relaxed so that less iterations are needed to complete an energy minimization. The resulting computation time savings could then be reinvested in treating large zeolite systems.

The choice in the functional representation of the electrostatic energetics is crucial to the magnitude of this energy contribution. This is clear from Table IV. However, the resultant geometries, using different electrostatic potential energy representations, are virtually identical. This can be inferred from Table IV by noting that each energy contribution, other than the electrostatic term, has about the same energy value for each of the three electrostatic models employed.

The major finding from the ion binding calculations involves the location of the cage oxygens. The characteristic binding energies and geometries are both dependent upon the geometry of the cage oxygens. An implication of this finding is that the oxygens can facilitate or retard binding and/or transport of mobile species by adopting correspondingly appropriate geometric states. For positive ions the cage oxygen can come out of the plane of sodalite faces in order to electrostatically attract the ion.

The aluminum atoms exhibit minor effects on the binding of the ions to the 12-membered ring surface of a sodalite cage. The flexibility of cage oxygens, and the corresponding implication to intermolecular electrostatic bonding interactions, far outweighs the interactions involving the heavy atoms of the sodalite cage. This finding is supporting evidence that the primary consequence of incorporating Al atoms into a sodalite cage is to stabilize (lower the energy) the cage.

Figure 7 provides information about how mobile ion binding depends upon aluminum atom content in a sodalite cage. For the Al-containing sodalite cages, the distribution of Al atoms is skewed on the side of the cage corresponding to negative values of d. This skewed Al atom distribution results in a maximum increase (compared to the all-Si structure) in Na^+ binding to the Al-rich 12-membered face of about 2 kcal/mol. Correspondingly, the Al-deficient 12-membered face on the opposite side of cage loses (relative to the all-Si structure) about 2.5 kcal/mol. These changes in ion binding energy are small in comparison to those realized from changes in oxygen geometry as is discussed in the next paragraph.

A uniformly symmetric cage oxygen geometry substantially lowers (stabilizes) the binding of the mobile ions to the sodalite cage. This is in contrast to a cage structure having nonequivalent geometric oxygens. A comparison of the binding curves of Figure 4 (asymmetric oxygens prior to energy minimization) and Figure 5 (symmetric oxygens after energy minimization) illustrates this finding. This behavior suggests that the strength of ion-binding to a sodalite cage is strongly dependent upon the geometric symmetry of its composite set of oxygens.

A higher level of simulation modeling is called for to further evaluate the flexibility of sodalite cage geometry. We hope to carry out both Monte Carlo and molecular dynamics calculations on a sodalite cage with the goal of characterizing molecular flexibility. Also, we need to more fully explore the nature of intercage interactions and their role on zeolite geometry. This means treating larger molecular assemblies which should not be a problem other than an increase in computing time. In this regard, the current study of the complete structural optimization of a sodalite cage represents a trade-off to a constrained optimization of a sodalite framework model, that is, multiple sodalite

cages. The current investigation probes the local geometry of the sodalite cage in detail, at the expense of longer range interactions such as pseudo-modeling energy contributions inherent to different frameworks composed of sodalite cages.

Acknowledgment. We greatly acknowledge the helpful interactions and discussions with Dr. Stelian Grigoras of Dow Corning Corp. and Dr. H. W. W. Tsao, and his colleagues, at Sun Refining and Marketing Co.

Properties of Atoms in Molecules: Atomic Volumes

Richard F. W. Bader,* Marshall T. Carroll, James R. Cheeseman, and Cheng Chang

Contribution from the Department of Chemistry, McMaster University, Hamilton, Ontario, Canada L8S 4M1. *Received May 1, 1987*

Abstract: The theory of atoms in molecules defines an atom and the average values of its properties. The intersection of an atomic surface, as defined by a property of the charge density, with a particular envelope of the charge density defines the volume of an atom in a molecule. The value of the density envelope used to bound the "open" portion of an atomic region can be chosen on the basis of comparison with measured properties. The nature of the results are, in any event, independent of the choice for envelopes which contain over 96% of the total electronic charge and lie within the usual range of van der Waals contact distances. It is shown that the volumes of methyl and methylene groups in normal hydrocarbons are transferable properties, as are their charge distributions, populations, and energies. The volume of a carbon atom subject to steric crowding is found to decrease as its stability and electron population increase. This behavior is opposite to that found for a carbon atom in a system with geometric strain as found in cyclic and bicyclic molecules. The stability, population, and volume of a carbon atom all undergo parallel increases as the atom is subjected to an increasing degree of geometric strain. The volumes of the bridgehead carbon atoms in bicyclo[1.1.0]butane and [1.1.1]propellane are 1.2 and 1.5 times, respectively, the volume of a methyl carbon atom. As anticipated on the basis of the orbital model, an increase in geometric strain is correlated with an increase in s character and thus one finds the electron population, stability, and volume of a carbon atom to undergo the same parallel increases in value through the series ethane, ethylene, acetylene. As a first step in the investigation of how atoms fit together, the changes in the atomic volumes accompanying the formation of a hydrogen bond are determined. The changes in volume are correlated with the changes in the atomic populations and energies for the formation of homo and hetero dimers of water and ammonia and their protonated species.

I. Introduction

It was pointed out by Bragg in 1920[1] that one can model a crystal through a representation of its atoms by spheres with characteristic radii, the radii being determined empirically from a body of experimental measurements so that the spheres of bonded atoms will be in approximate contact. This observation was followed by the establishment of sets of atomic (ionic) radii by a number of workers—Goldschmidt, Pauling, Zachariasen, and Slater as outlined in Slater's book on solids.[2] The idea of representing the spatial structure and extent of a system by centering "atomic" spheres of fixed radii at the experimentally determined average positions of the nuclei has been extended to systems other than crystals and is used for purposes other than accounting for or predicting crystal structures. Properties that one attempts to determine using the "atomic hard-sphere model" are the shape of a molecule, the volume it occupies, and the associated surface area. Bondi[3,4] calls the volume occupied by a molecule, that is, the volume impenetrable to other molecules, the van der Waals volume and the corresponding radii of the atomic spheres the van der Waals radii. The radii determined by van der Waals contact distances between molecules as required to recover packing densities of liquids and solids, kinetic collision cross sections, and other properties of the liquid state[3,4] result in spheres which overlap one another for neighboring atoms. Numerous algorithms have been proposed which take the common volume of overlapping atomic spheres into account in the calculation of the molecular volume. The scheme proposed by Gavezzotti[5] has been used to calculate the volumes of cavities in cage compounds and crystalline matrices and in the analysis of steric factors influencing reactions in the solid state.

The hard-sphere model has been useful in determining permissible peptide chain conformations.[6] Richards[7] has used the hard-sphere model to consider the packing of groups of atoms in proteins and the area of solvent–protein interfaces. The shape and area of the exposed surface of a molecule vary with the dimensions of the molecule used to probe its surface, reaching a limiting value as the size of the probe increases. Because of this problem, Richards has distinguished between the van der Waals envelope, the outer surface as determined by the hard-sphere model, the accessible surface, the continuous sheet defined by the locus of the center of the probe molecule as it rides over the van der Waals surface, the contact surface, those parts of the van der Waals surface that are actually in contact with the surface of the probe, and the reentrant surface, as defined by the interior facing part of the probe when it is simultaneously in contact with more than one atom. The latter two surfaces combine to form a continuous sheet which is a possible definition of the molecular surface, a surface termed the solvent-accessible surface by Connolly.[8] This author calculates the solvent-excluded volume of a molecule by a direct determination of the volume enclosed by the solvent-accessible surface, the surface, and its area being determined by an analytical procedure. This method is more accurate than previous ones because of its analytical treatment of the surface

(1) Bragg, W. L. *Phil. Mag.* **1920**, *40*, 169.
(2) Slater, J. C. *Quantum Theory of Molecules and solids*; McGraw-Hill: New York, 1925; Vol. 2, p 95.
(3) Bondi, A. *J. Phys. Chem.* **1964**, *68*, 441 (1964).
(4) Bondi, A. *Physical Properties of Molecular Crystals, Liquids and Glasses*; Wiley: New York, 1968.
(5) Gavezzotti, A. *J. Am. Chem. Soc.* **1983**, *105*, 5220; **1985**, *107*, 962.
(6) Ramachandran, G. N.; Sasisekharan, V. *Adv. Protein Chem.* **1968**, *23*, 284.
(7) Richards, F. M. *Annu. Rev. Biophys. Bioeng.* **1977**, *6*, 151.
(8) Connolly, M. L. *Science* **1983**, 221, 709; *J. Am. Chem. Soc.* **1985**, *107*, 1118.

0002-7863/87/1509-7968$01.50/0